WARSAW UNIVERSITY OF TECHNOLOGY Index 351733
FACULTY OF CIVIL ENGINEERING
COMMITTEE FOR CIVIL AND WATER ENGINEERING
POLISH ACADEMY OF SCIENCES ISSN 1230-2945
DOI: 10.24425/ace.2020.136476
ARCHIVES OF CIVIL ENGINEERING
Vol. LXVII ISSUE 1 2021

BUCKLING RESISTANCE OF QUASI-STRAIGHT H-SECTION BEAM-COLUMNS UNDER UNEQUAL END MOMENTS

M.A. GIŻEJOWSKI[1], R.B. SZCZERBA[2], Z. STACHURA[3], M.D. GAJEWSKI[4]

Steel prismatic elements of equal flanges double-tee section subject to major axis bending and compression, unrestrained in the out-of-plane direction between the supports, are vulnerable to buckling modes associated with minor axis flexural and torsional deformations. When end bending moments are acting alone on the quasi-straight member, the sensitivity to lateral-torsional buckling (LTB) is very much dependent upon the ratio of section minor axis to major axis moments of inertia, and additionally visibly dependent upon the major axis moment gradient ratio. In the case of major axis bending with the presence of a compressive axial force, even of rather small value in relation to the section squash resistance, there is a drastic reduction of structural elements in their realistic lengths to maintain a tendency to fail in the out-of-plane mode, governed by the large twist rotation. Increasing the load effects ratio of dimensionless axial force to dimensionless maximum major axis bending moment, the buckling mode goes away from that of lateral-torsional one, starting to become that closer to the minor axis flexural buckling (FBZ) mode. Different aspects of the flexural-torsional buckling (FTB) resistance of the typical rolled H-section beam-column with regard to the General Method (GM) formulation, developed by the authors elsewhere and based on the parametric finite element analysis, are dealt with in this paper. Investigations are concerned with different member slender ratio, different moment gradient ratios and different load effects ratio. Final conclusions are related to practical applications of the proposed format of General Method in relation to the effect of large displacements on the FTB resistance reduction factor described through the dimensionless measure of action effects and the FTB relative slenderness ratio of quasi-straight beam-columns.

Keywords: General Method, large displacements, flexural-torsional buckling, steel rolled H-section, beam-column

[1] Prof., DSc., PhD., Eng., Warsaw University of Technology, Faculty of Civil Engineering, Al. Armii Ludowej 16, 00-637 Warsaw, Poland, e-mail: m.gizejowski@il.pw.edu.pl

[2] MSc., Eng., Warsaw University of Technology, Faculty of Civil Engineering, Al. Armii Ludowej 16, 00-637 Warsaw, Poland, e-mail: r.szczerba@il.pw.edu.pl

[3] MSc., Eng., Warsaw University of Technology, Faculty of Civil Engineering, Al. Armii Ludowej 16, 00-637 Warsaw, Poland, e-mail: z.stachura@il.pw.edu.pl (corresponding author)

[4] DSc., PhD., Eng., Warsaw University of Technology, Faculty of Civil Engineering, Al. Armii Ludowej 16, 00-637 Warsaw, Poland, e-mail: m.gajewski@il.pw.edu.pl

1. INTRODUCTION

The flexural-torsional buckling of laterally and torsionally unrestrained beam-columns is one the most important failure modes need to be considered in design of steel framework elements. The current design regulations presented in Part 1-1 of Eurocode 3 implemented in Poland as PN-EN 1993 [6], introduce buckling strength interaction equations of clause 6.3.3 for checking the resistance utilization ratio of beam-columns under a triple action effect of compression and bending moments about both section principal axes *y-y* and *z-z*. The said equations are also valid for all special cases of a single action effect of major axis bending, minor axis bending or compression, and for a double action effect of biaxial bending without compression, and compression with mono-axial bending about *y-y* axis or *z-z* axis, as it has been explained in the Eurocode 3 Design Manual [18]. For a double action effect of compression and bending, the most important case in practical design is the major axis bending since majority of frameworks are still designed with use of plane frame models. In Eurocode 3 [6], the rules based on interaction equations of clause 6.3.3 are supplemented with recommendations based on the so-called General Method (GM) of clause 6.3.4. An idea of GM introduced in [6] is to bring the checking method for beam-columns closer to the Ayrton-Perry verification procedure of columns and beams, requiring a single verification criterion instead of triple criteria, two based on the buckling interaction equations with the so-called equivalent uniform moment factors and the criterion of cross section resistance. Although the GM version implemented in [6] has a general format of that of Ayrton-Perry for compression or major axis bending (based on the conventional definition of minor axis flexural slenderness ratio $\bar{\lambda}_z$ or the lateral-torsional slenderness ratio $\bar{\lambda}_{LT}$, respectively), it does not follow the same way of imperfection inclusion as that used for compression or bending. The effect of imperfection is not implemented through the interpolation of equivalent imperfection amplitude for beam-columns from those for buckling under compression and for buckling under major axis bending. It is recommended to calculate the beam-column strength reduction factor through the adoption, alternatively [18]: a) the minimal value of the reduction factors calculated for compression χ_z and bending χ_{LT}, both based on the calculated beam-column slenderness ratio $\bar{\lambda}_{op}$ (denoted hereafter by $\bar{\lambda}_{FT}$), or b) the value being interpolated between the above mentioned two by using a relationship that is dependent upon the action effects ratio (dimensionless axial force over the dimensionless maximum bending moment).

The Ayrton-Perry version of Eurocode's GM is not fully aligned with the original version of Ayrton-Perry concept, and this inconsistency has recently been widely studied. The information on the

application of the GM can be found in [15, 18]. Comparison of the GM with the other rules given in [6] was made in [4, 24]. Ferreira et al. [7] compared the GM with other overall methods. The safety of this method was assessed in [17] for prismatic members and with the use of advanced nonlinear numerical simulations. Recent international research is more frequently based on a direct application of the Ayrton-Perry approach. Tankova et al. [23] presented an Ayrton-Perry format proposal for beam-columns based on the theoretical derivation of [21]. Other proposals were reported in [14, 22]. A novel analytical GM model based on a generalised Ayrton-Perry formulation was proposed by the authors of this paper in [9].

In this paper, GM is studied in relation to quasi-straight wide flange beam-columns subjected to unequal end moments giving the moment gradient ratio $\psi_y = M_{y,min}/M_{y,max}$. Similar study but related to lateral-buckling of quasi-straight double-tee section beam-columns, under compression and uniform bending ($\psi_y = 1$), was presented in [10]. Straight and residual stress free beams (when end moments do not exist) are more sensitive to LTB when the ratio of minor axis to major axis moments of inertia is closer to zero (for the section shape being closer to the thin web plate without flanges) while less sensitive otherwise, and ultimately insensitive to LTB in the case of double-tee section beams with equal moments of inertia about both principal axes. Quasi-perfect inelastic beams with an infinitesimally small value of the amplitude of geometric imperfection profile fail in: a) plastic in-plane mode with limited contribution of the twist rotation (the range of stocky beams), b) quasi-elastic mode combining the effects of out-of-plane deformations with prebuckling deflections (the range of intermediate lengths), and finally c) plastic out-of-plane mode (the range of slender beams). In the other words, the buckling failure mode changes with an increase of the beam length, from that of the plastic major axis failure, governed almost entirely by large in-plane deformations, through the mode associated with an increasing contribution of the minor axis bending as a result of the development of quasi-elastic out-of-plane deformations, to finally that of the minor axis failure, governed almost entirely by large minor axis plastic deformations as a result of large twist rotations. In the case of major axis bending with the presence of a compressive axial force, even of a small value, there is a drastic reduction for structural elements in their realistic lengths to maintain a tendency to fail in the out-of-plane mode governed by the large twist rotation. The objective of this paper is twofold. Firstly, to prove that regardless of the moment gradient ratio, the GM buckling resistance reduction factor of quasi-straight and residual stress free beam-columns may be represented, except for the values for low beam-columns slenderness ratio $\bar{\lambda}_{FT}$, by the elastic buckling hyperbola $\frac{1}{\bar{\lambda}_{FT}^2}$. Secondly, to confirm that the large twist rotation affecting the resistance of very slender beams by increasing the resistance

above that resulting from the elastic buckling hyperbola, might be considered as negligible when the major axis bending moment is accompanied by a small axial force.

2. FINITE ELEMENT SIMULATIONS

Let us consider a simply supported beam-column with free warping boundary conditions at end sections of the wide flange rolled section HEB 300 made of steel grade S 235, under compression and major axis end moments (Fig. 1). Three loading cases of beam-columns are considered in this paper, namely $\psi_y = 1, 0, -1$. The parametric finite element simulations were carried out for the fourteen values of minor axis flexural slenderness ratio $\bar{\lambda}_z = \sqrt{\frac{N_{pl}}{N_z}}$ (where N_z is the flexural minor axis bifurcation force according to [6, 18]) where $\bar{\lambda}_z$ = 0.5; 1.0; 1.5; 2.0; 2.5; 3.0; 4.0; 5.0; 6.0; 7.0; 8.0; 9.0; 12.0; 16.0, and twelve values of the action effects ratio $\alpha_{n,y} = n/m_y$ (or $\alpha_{m,y} = m_y/n = 1/\alpha_{n,y}$) where $\alpha_{n,y}$ = 0; 1/50; 1/20; 1/10; 1/4; 1/2; 3/4; 0.0; 4/3; 2; 4; ∞ (or $\alpha_{m,y}$ = ∞; 50; 20; 10; 4; 2; 4/3; 0.0; 3/4; 1/2; 1/4; 0). For the moment gradient ratio $\psi_y = 1$, the slenderness ratio $\bar{\lambda}_z$ = 0.5-6.0 and the action effects ratio $\alpha_{n,y}$ without values 1/50; 1/20; 1/10 are considered. For the moment gradient ratio $\psi_y = 0$ the slenderness ratio $\bar{\lambda}_z$ = 0.5-12.0 and all of the action effects ratio $\alpha_{n,y}$ are considered. In case of antisymmetric major axis bending moment ($\psi_y = -1$), all of $\bar{\lambda}_z$ and $\alpha_{n,y}$ are considered. The dimensionless action effects are defined by: $n = \frac{N}{N_{pl}}$, $m_y = \frac{M_{y,max}}{M_{y,pl}}$ where the section plastic resistances: $N_{pl} = Af_y$, $M_{y,pl} = W_{y,pl}f_y$; A, $W_{y,pl}$ – section area and section plastic modulus, f_y – steel yield stress.

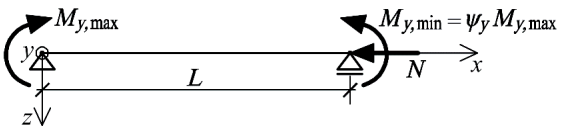

Fig. 1. Loading pattern of considered beam-column of HEB 300 cross-section

The finite element model is obtained by geometric discretization of section walls with use of shell elements S4R (a 4-node doubly curved thin or thick shell, reduced integration, hourglass control, finite membrane strains). The mesh density adopted was chosen such that it insures the convergence of the equilibrium path trace and the limit point placement on this path. The shell finite element size changes, depending on the beam-column length, with the dimension being constant along the mid-

thickness line of section walls (30 mm for the flanges and 28 mm for the web) and variable along the member axis of 50 mm on average. The boundary conditions for end sections are modelled using rigid sub-contours for two flanges and one sub-contour for the web with shell elements multipoint constrained. The web sub-contour is "hinged" to the rigid flange contours so that the former would rotate in the section plane independently from the other two. Hence, the flange sub-contour rotation in the section plane is constrained at the flange-to-web intersection so that the flange sub-contours may freely rotate only out of the section plane, ensuring warping conditions as in the Vlasov theory of thin-walled members, but all the sub-contours are restricted to differential rotations in the section plane. Such a shell modelling technique facilitates the introduction of end section translational and rotational boundary conditions, as well as the application of external concentrated loads, in the same way as in the Vlasov theory of thin-walled members. Details are shown in Fig. 2.

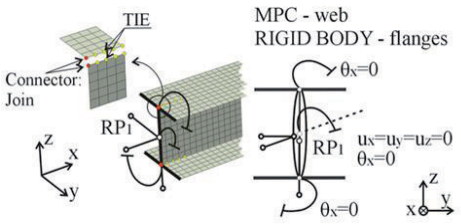

Fig. 2. Numerical model details: end boundary conditions

The elastic-plastic behaviour of steel is modelled assuming Hooke's relationship for isotropic material in the linearity range while for detection of plastic behaviour the Huber-Mises yield condition is applied [13, 20]. After crossing the yield condition the plastic strains are determined on the basis of flow rule associated with chosen yield condition and isotropic strain hardening model is applied to describe material's behaviour after plasticization. The elasto-plasticity constitutive model parameters are calibrated on the basis of a trilinear engineering stress-strain relationship illustrated graphically in Fig. 3, in which the first line represents the region of elastic behaviour, the second one the region of inelastic linear behaviour between the yield stress f_y and the tensile strength of $f_u = 1.1\ f_y$ at the strain of $\varepsilon_u = 0.15$ %, followed by the constant tensile stress under the strain increased above the level of $\varepsilon_u = 0.15$ %. For the elasticity the assumed Young's modulus value for steel is equal to $E = 210 \cdot 10^3$ N/mm^2 while Poison's ratio is equal to 0.3.

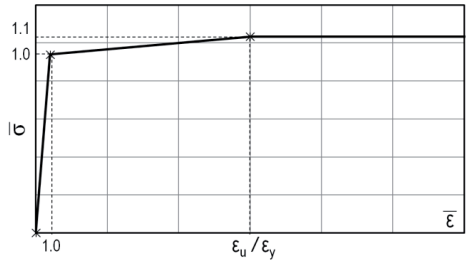

Fig. 3. Stress-strain relationship adopted for modelling of steel behaviour, f_y = 235 MPa

Abaqus finite element code is used to solve the problems of linear eigenvalue analysis (LEA) for elastic buckling mode and geometrically and materially nonlinear analysis with a disturbance to perfect geometry (GMNA+) in the form of infinitesimally small minor axis end moments that produce the initial configuration corresponding to the lowest buckling mode [1, 2]. Exemplary lowest overall buckling modes for the slenderness ratio $\bar{\lambda}_z$ = 5.0 and specified dimensional n and m_y values are given in the Appendix.

The option Nlgeom is used that allows for the nonlinear buckling analysis through the large deformation theory [5]. The engineering stress-strain relationship is transformed into the true stress and true strain relationship according to approximate relations given in manual [2]. The Riks incremental-iterative method is used to solve all the GMNA+ problems related to compression and uniform, symmetric major axis bending moment (SMY), compression and triangular major axis bending moment (TMY) and bi-triangular, antisymmetric major axis bending moment (AMY).

It is worth underling here that the FEM approach used as a base for all calculations presented in this paper was verified/validated in the previous authors' contributions [8, 9, 11]. In fact, the approach was not validated with use of the authors' original experiments, but rather was based on experiments accessible in the subject literature. What is more important, such an approach has additionally been verified many times by checking with analytical models meeting the current steel Eurocodes' Expectations (ECE).

2.1 RESULTS FOR UNIFORM BENDING MOMENT (SMY)

The results of finite element simulations of the buckling resistance $M_b = \chi_{LT} M_{y,pl}$ are shown in Fig. 4 in the form of multiple buckling moment reduction factor curves under the simultaneous action of the bending and axial compression load effects, each curve representing the buckling moment

reduction factor $\chi_{LT} = \frac{M_b}{M_{y,pl}}$ and the lateral-torsional (LT) slenderness $\bar{\lambda}_{LT} = \bar{\lambda}_{LT,ref} = \sqrt{\frac{M_{y,pl}}{M_{cr,LEA}}}$ where $M_{cr,LEA}$ is the critical moment according to the beam theory of thin-walled members:

(2.1) $$M_{cr,LEA} = i_0\sqrt{N_z N_T} = \frac{i_0 N_{pl}}{\bar{\lambda}_z \bar{\lambda}_T}$$

where:

i_0 – section polar radius of gyration; N_z, N_T – bifurcation forces corresponding to minor axis flexural buckling and torsional buckling modes, respectively; $\bar{\lambda}_z$, $\bar{\lambda}_T$ – relative slenderness ratios corresponding to above stated bifurcation forces [18].

The LT slenderness ratio can be modified with regard to the effect of prebuckling displacements [11], following the notation $\bar{\lambda}_{LT,\mathrm{mod}} = \sqrt[4]{1 - I_z/I_y}\,\bar{\lambda}_{LT}$ where I_z and I_y are the moments of inertia about the *z*-*z* and *y*-*y* axes, respectively.

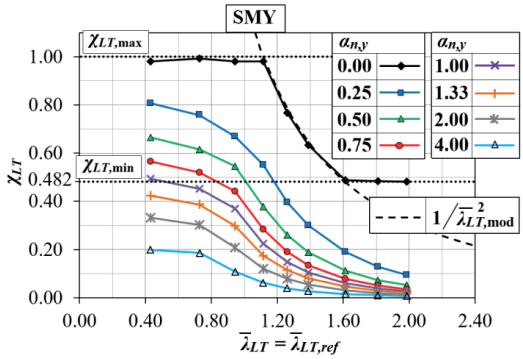

Fig. 4. FEM buckling reduction factor vs. the LT slenderness ratio for the case of SMY [10]

Figure 4 shows that for uniform bending without compression ($\alpha_{n,y} = 0$), numerical results coincide with the upper bound of elastic-plastic instability in the wide range of $\bar{\lambda}_{LT}$. The upper bound is constituted by minimum from the values of elastic hyperbola (dashed line) and plastic hinge resistance (dotted line) at the level of $\chi_{LT} = \chi_{LT,max}$ where $\chi_{LT,max} = 1$. The level of minor axis failure of slender beams, at the twist rotation amplitude of 90 degrees, corresponds to $\chi_{LT,min} = M_{z,pl}/M_{y,pl} = 0.482$. This level is marked in Fig. 4 by the dotted lower bound line at the level of $\chi_{LT} = \chi_{LT,min}$. It is visible that for slender beams with the slenderness ratio $\bar{\lambda}_{LT}$ greater than

$\bar{\lambda}_{LT,max} \approx 1.6$, the buckling reduction factor starts to approach the constant value of $\chi_{LT,min}$. When there is the bending moment accompanied by the compressive axial force, buckling reduction factor curves are placed below that for the bending moment without compression. For stocky beam-columns the buckling resistance reduction factor starts to decrease from that of $\chi_{LT} = M_{y,pl,red}/M_{y,pl}$ (where $M_{y,pl,red}$ is the section plastic moment resistance reduced by the presence of axial force) and the curves are located below that for bending without compression. The position is lower for the greater value of the action effects ratio of $\alpha_{n,y}$. One can notice that the range of constant level of the buckling reduction factor vanishes for slender beam-columns.

2.2 RESULTS FOR TRIANGULAR BENDING MOMENT (TMY)

The FEM simulation results for TMY case are shown in Fig. 5. The slenderness ratio is calculated using the critical moment $M_{cr,LEA}$ according to the beam theory of thin-walled members:

$$M_{cr,LEA} = 1.82 i_0 \sqrt{N_z N_T} = 1.82 \frac{i_0 N_{pl}}{\bar{\lambda}_z \bar{\lambda}_T} \tag{2.2}$$

where there is the same notation as used in Eqn. (2.1).

It shows that for bending without compression ($\alpha_{n,y} = 0$), due to the major axis moment applied over one support, the numerical results coincide with the upper bound of elastic hyperbola only in a narrow range of $\bar{\lambda}_{LT}$ between approximately 1.15 and 1.4. For $\bar{\lambda}_{LT}$ below unity, numerical results are placed above the plastic hinge level of $\chi_{LT} = \chi_{LT,max}$ where $\chi_{LT,max} = 1$. This indicates that the effect of strain hardening is influencing the in-plane resistance of stocky beams much more in the case of non-uniform bending than in the case of uniform bending. It is also visible that for slender beams with the slenderness ratio $\bar{\lambda}_{LT}$ greater than $\bar{\lambda}_{LT,max} \approx 1.4$, there is a similar tendency to that observed in the case of SMY. The buckling reduction factor starts to approach the constant value of $\chi_{LT,min}$. When there is the bending moment accompanied by the compressive axial force, buckling reduction factor curves are placed below that for the bending moment without compression as it has been observed for uniform bending and compression (cf. subsection 2.1).

Figure 6 shows the comparison of FEM results for different values of $\alpha_{n,y}$ in the cases of SMY and TMY. For the reference, there are also shown the results from FEM simulations for the case of $\alpha_{n,y} = 0$. One can notice that for all the values of the slenderness ratio considered, buckling moment reduction factors for TMY are placed above those for SMY but the difference is the decreasing function of the

slenderness ratio. This is due to the fact that the effect of strain hardening is much more pronounced for stocky elements in the case of TMY than in the case of SMY. This conclusion supports the remarks made by the authors of this study in [9]. The effect of strain hardening plays more and more important role when the bending moment diagram goes from that corresponding to SMY to the one corresponding to AMY.

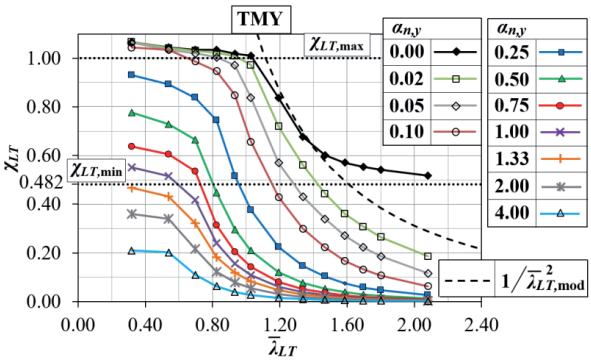

Fig. 5. FEM buckling reduction factor vs. the LT slenderness ratio for the case of TMY

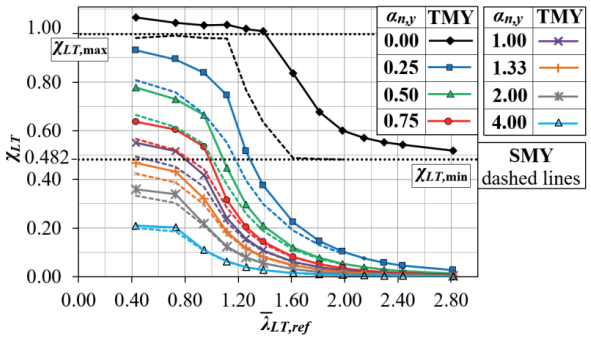

Fig. 6. Comparison of buckling reduction factor function of LT slenderness ratio for the cases of SMY and TMY

2.3 RESULTS FOR BI-TRIANGULAR BENDING MOMENT (AMY)

The FEM simulation results for AMY case are shown in Fig. 7. The slenderness ratio is calculated using the critical moment $M_{cr,LEA}$ according to the beam theory of thin-walled members:

(2.3) $$M_{cr,LEA} = 2.64 i_0 \sqrt{N_z N_T} = 2.64 \frac{i_0 N_{pl}}{\bar{\lambda}_z \bar{\lambda}_T}$$

where there is the same notation as used in Eqns. (2.1) and (2.2).

It shows that for bending due to the moments of the same direction and applied over both supports without compression ($\alpha_{n,y} = 0$), the numerical results coincide with the upper bound of elastic hyperbola only in a narrow range of $\bar{\lambda}_{LT}$ being approximately similar to that identified in the case of TMY. For $\bar{\lambda}_{LT}$ below unity, numerical results are placed above the plastic hinge level of $\chi_{LT} = \chi_{LT,max}$ where $\chi_{LT,max} = 1$. It is visible that for slender beams with the slenderness ratio $\bar{\lambda}_{LT}$ greater than $\bar{\lambda}_{LT,max} \approx 1.4$, there is a similar tendency to that observed in the cases of SMY and TMY. The buckling reduction factor starts to approach the constant value of $\chi_{LT,min}$.

Figure 8 shows the comparison of FEM results for different values of $\alpha_{n,y}$ in the cases of TMY and AMY. For the reference, there are also shown the results from FEM simulations for the case of $\alpha_{n,y} = 0$. One can notice that for all the values of the slenderness ratio considered, buckling moment reduction factors for AMY are placed above those for TMY but the difference for stocky beam-columns is not so much pronounced as it exists when comparing the results of TMY and SMY (cf. Fig. 6). This is due to the fact that the effect of strain hardening is similar for non-uniform bending cases TMY and AMY than that between the uniform moment case SMY and the non-uniform bending cases TMY and AMY.

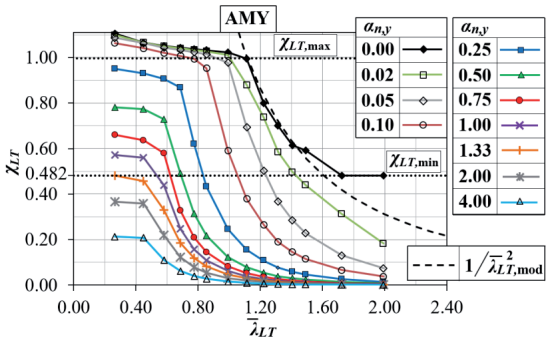

Fig. 7. FEM buckling reduction factor vs. the LT slenderness ratio for the case of AMY

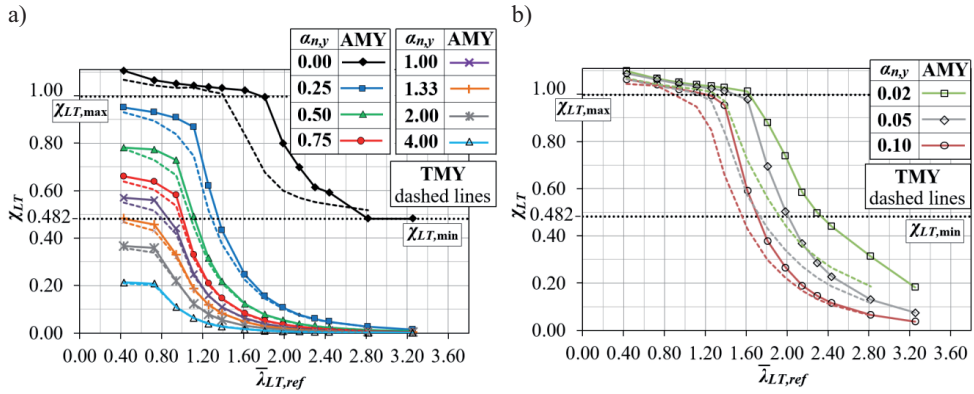

Fig. 8. Comparison of buckling reduction factor function of LT slenderness ratio for the cases of TMY and AMY: a) $\alpha_{n,y} = 0.00$ and $\alpha_{n,y} \geq 0.25$; b) $\alpha_{n,y} = 0.02$, 0.05 and 0.10

3. BUCKLING RESISTANCE BY GENERAL METHOD IN AYRTON-PERRY FORMAT

The GM concept of the buckling resistance assessment developed in [9] enabled to extend the Ayrton-Perry approach used for the resistance assessment of the member under a single load effect (N_b when the member is subject to a compressive force N or M_b when it is subject to a bending moment M_y) for the assessment of the member resistance under a combination of the load effects of N and M_y. In order to do that, an Euclidean dimensionless measures are introduced, referred respectively to the actual member state and the buckling resistance state:

(3.1) $$s = \sqrt{n^2 + m_y^2}$$

(3.2) $$s_b = \sqrt{n_b^2 + m_b^2}$$

where:

$n = N/N_{pl}$, $m_y = M_y/M_{y,pl}$, $n_b = N_b/N_{pl}$, $m_b = M_b/M_{y,pl}$ and each pair of measures represented by Eqns. (3.1) and (3.2) are associated with the same action effects ratio of $\alpha_{n,y}$ or $\alpha_{m,y} = m_y/n = 1/\alpha_{n,y}$.

Numerical results presented in the previous chapter may be effectively used for the evaluation of the member buckling resistance measure s_b. Connecting discrete values $s_{b,i}$ calculated for the selected

value of the slenderness ratio $\bar{\lambda}_z$ and different values of $\alpha_{n,y}$ or $\alpha_{m,y}$ (from zero to unity), the buckling resistance measure curve may be obtained. Fig. 9 shows these curves obtained for three moment gradient ratios, namely in Fig. 9 for SMY, in Fig. 10 for TMY and in Fig. 11 for AMY. In each figure there is a number of curves for different values of the slenderness ratio values $\bar{\lambda}_z$ used in FEM simulations.

The slenderness ratio either $\bar{\lambda}_z$ used in Fig. 9 or $\bar{\lambda}_{LT}$ used in chapter 2, are not of a general nature, since they are associated with independent buckling modes. In order to formulate the buckling resistance measure curve in the same way like for compression and bending, the following two measures are introduced:

(3.3) $$s_{cr} = \sqrt{n_{cr}^2 + m_{cr}^2}$$

(3.4) $$s_{pl}^{II} = \sqrt{n_{pl}^2 + m_{pl}^2}$$

where:

$n_{cr} = N_{cr}/N_{pl}$, $m_{cr} = M_{cr}/M_{y,pl}$ – pair of the dimensionless values of compressive force and bending moment at the elastic critical state, and $n_{pl} = N/N_{pl}$, $m_{pl} = M_y/M_{y,pl}$ – pair of the dimensionless compressive force and bending moment (satisfying Eqn. (3.8) where $P - \delta_z$ effect is accounted for the moment evaluation) at the in-plane ultimate strength reached when the plastic hinge forms at the most stressed section.

Using Eqns. (3.3) and (3.4), the following definitions for the flexural-torsional buckling resistance measure and the flexural-torsional buckling slenderness ratio are introduced:

(3.5) $$s_b = \chi_{FT} s_{pl}^{II}$$

(3.6) $$\bar{\lambda}_{FT} = \sqrt{\frac{s_{pl}^{II}}{s_{cr}}}$$

where:

$\chi_{FT} = s_b/s_{pl}^{II}$ – flexural-torsional buckling reduction factor.

It is important to notice that for compression without bending ($\alpha_{n,y} = 0$ or $\alpha_{m,y} = \infty$) there is $s_b = N_b/N_{pl}$ and for bending without compression ($\alpha_{m,y} = 0$ or $\alpha_{n,y} = \infty$) there is $s_b = M_b/M_{y,pl}$. In order to present the results of FEM simulations in the coordinate system of the flexural-torsional buckling reduction factor χ_{FT} and the flexural-torsional slenderness ratio $\bar{\lambda}_{FT}$, the critical action effects measure and the in-plane ultimate state action effects measure are studied first, and they are summarized in the following subsections.

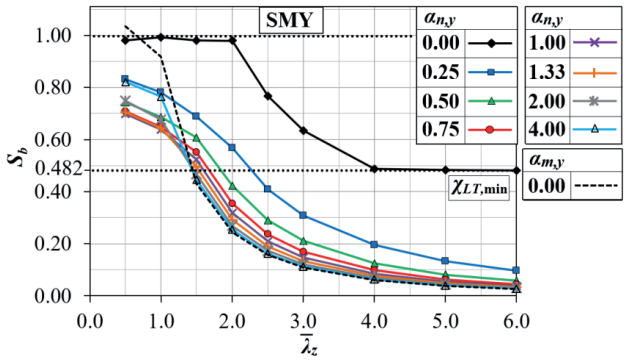

Fig. 9. Buckling resistance measure curves for SMY

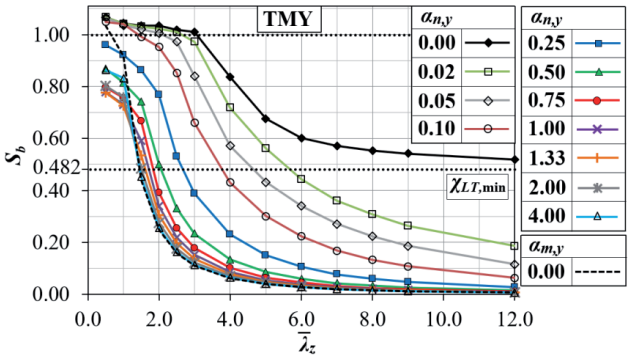

Fig. 10. Buckling resistance measure curves for TMY

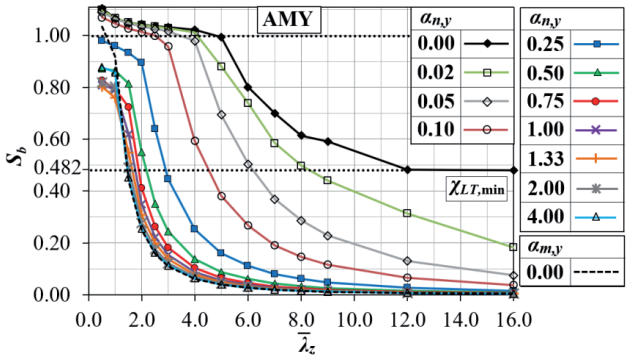

Fig. 11. Buckling resistance measure curves for AMY

3.1 CRITICAL ACTION EFFECTS MEASURE

The critical state of beam-columns under a moment gradient defined by ψ_y is described by the relationship used in [9] and rearranged to the following dimensionless formats:

$$\left(m_{cr}\bar{\lambda}^2_{LT,ref}\beta_{\mathrm{mod}}\right)^2 = \left(1 - n_{cr}\bar{\lambda}^2_y\right)\left(1 - n_{cr}\bar{\lambda}^2_z\right)\left(1 - n_{cr}\bar{\lambda}^2_T\right) \tag{3.7}$$

where:

$\bar{\lambda}_y$ – column slenderness ratios corresponding to flexural buckling about the y-y axis [6], β_{mod} – factor depends on the moment gradient ratio ψ_y and N/N_z and the effect of prebuckling in-plane displacements on the critical moment [9].

The critical state curves are evaluated from discrete points calculated for three values of ψ_y and the same slenderness ratio (in order to better represent the elastic critical state additionally $\bar{\lambda}_z$ = 0.6; 0.7; 0.8 were used) and action effects factor values as for numerical simulations. The results are presented in Fig. 12 for the case of SMY, in Fig. 13 for the case TMY and in Fig. 14 for the case of AMY.

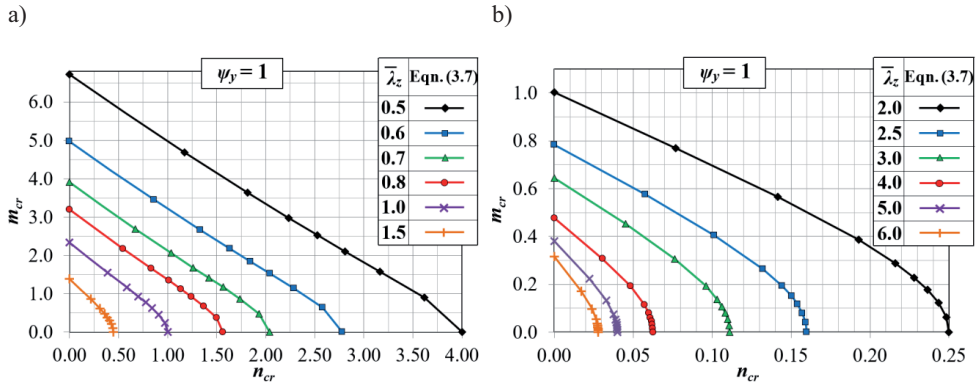

Fig. 12. Analytical elastic critical state curves for SMY [10]

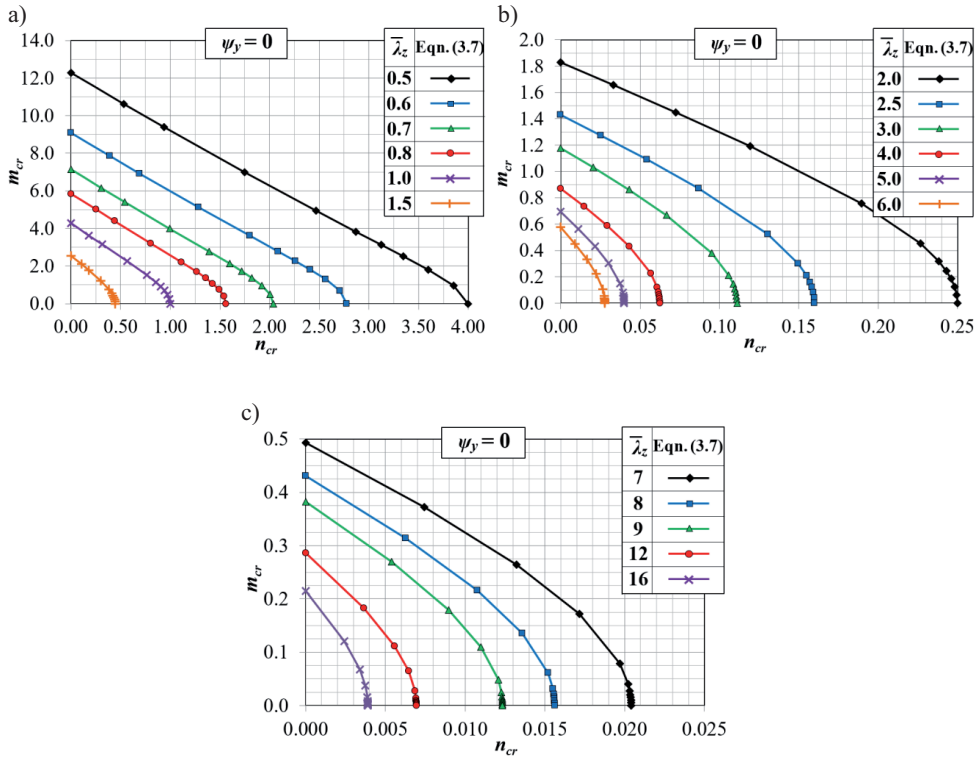

Fig. 13. Analytical elastic critical state curves for TMY

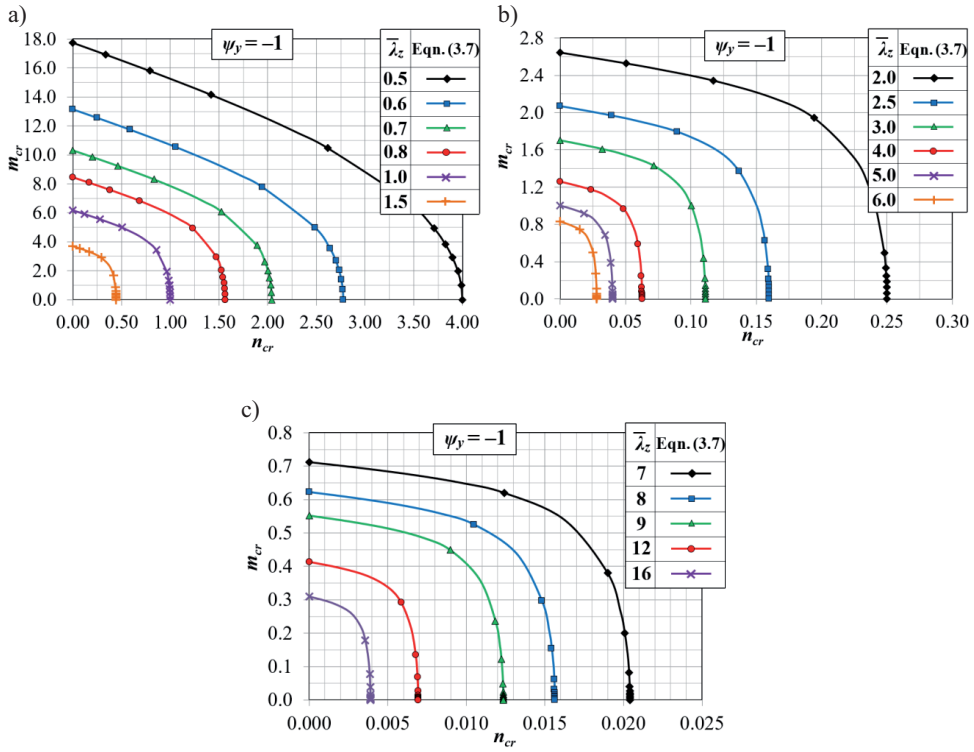

Fig. 14. Analytical elastic critical state curves for AMY

3.2 IN-PLANE ULTIMATE STATE ACTION EFFECTS MEASURE

The in-plane ultimate state of beam-columns under a moment gradient defined by ψ_y is widely presented in [8]. For this study, the relationships described in [19, 25] are used and rearranged to the following dimensionless formats:

- for $\bar{\lambda}_y \leq 1$:

a) when $\psi_y > cos\left(\pi\bar{\lambda}_y\sqrt{n_{pl}}\right)$

$$\frac{m_{pl}\sqrt{1+\left[cot\left(\pi\bar{\lambda}_y\sqrt{n_{pl}}\right)-\psi_y cosec\left(\pi\bar{\lambda}_y\sqrt{n_{pl}}\right)\right]^2}}{m_{N,y}} = 1 \tag{3.8a}$$

b) when $\psi_y \leq cos\left(\pi\bar{\lambda}_y\sqrt{n_{pl}}\right)$

(3.8b) $$\frac{m_{pl}}{m_{N,y}} = 1$$

- for $\bar{\lambda}_y > 1$:

a) when $\psi_y > cos\left(\pi\sqrt{n_{pl}}\right)$

(3.8c) $$\frac{m_{pl}\sqrt{1+\left[cot\left(\pi\sqrt{n_{pl}}\right)-\psi_y cosec\left(\pi\sqrt{n_{pl}}\right)\right]^2}}{m_{N,y}} = 1$$

b) when $\psi_y \leq cos\left(\pi\sqrt{n_{pl}}\right)$, Eqn. (3.8b) holds

where:

cot, *cosec* – trigonometric cosecant and cotangent function, respectively; $m_{N,y}$ – dimensionless section reduced moment resistance for bending about *y-y* axis according to Eqn. (3.9).

Eurocode's interaction criteria for the evaluation of section reduced moment resistance $m_{N,y}$ of steel double-tee sections subjected to axial force and bending about *y-y* axis generate unconservative results compared to the exact solution (which can be found in [26]), particularly for low values of n_{pl} [16]. The authors of paper [12] derive the bending moment - axial force interaction relations for mild steel bisymmetric I-sections by considering elastic-plastic and strain hardening idealisations with linear and parabolic strain hardening characteristics. Other modern alternative interaction criteria were given in [3, 19, 27]. For the purpose of this study, the proposal of [19] is taken into account since it is likely to be adopted for the future generation of Eurocode 3. The formula presented in [19] is rearranged to calculating $m_{N,y}$ and the following dimensionless format:

(3.9a) $$m_{N,y} = 1 - \frac{A^2}{4W_{y,pl}t_w}n_{pl}^2 \quad \text{for} \quad n_{pl} \leq \frac{A_w}{A}$$

(3.9b) $$m_{N,y} = \left(1 - n_{pl}\right)\frac{1-\frac{A_w^2}{4W_{y,pl}t_w}}{1-\frac{A_w}{A}} \quad \text{for} \quad n_{pl} > \frac{A_w}{A}$$

where:

$A_w = h_w t_w$; *A* – cross-section area; h_w – double-tee section mid-flange depth; t_w – web thickness.

In-plane resistance curves are evaluated from discrete points calculated for three values of ψ_y and the same slenderness ratio and action effects factor values as for numerical simulations. The results are presented in Fig. 15 for all considered cases of the moment gradient ratio.

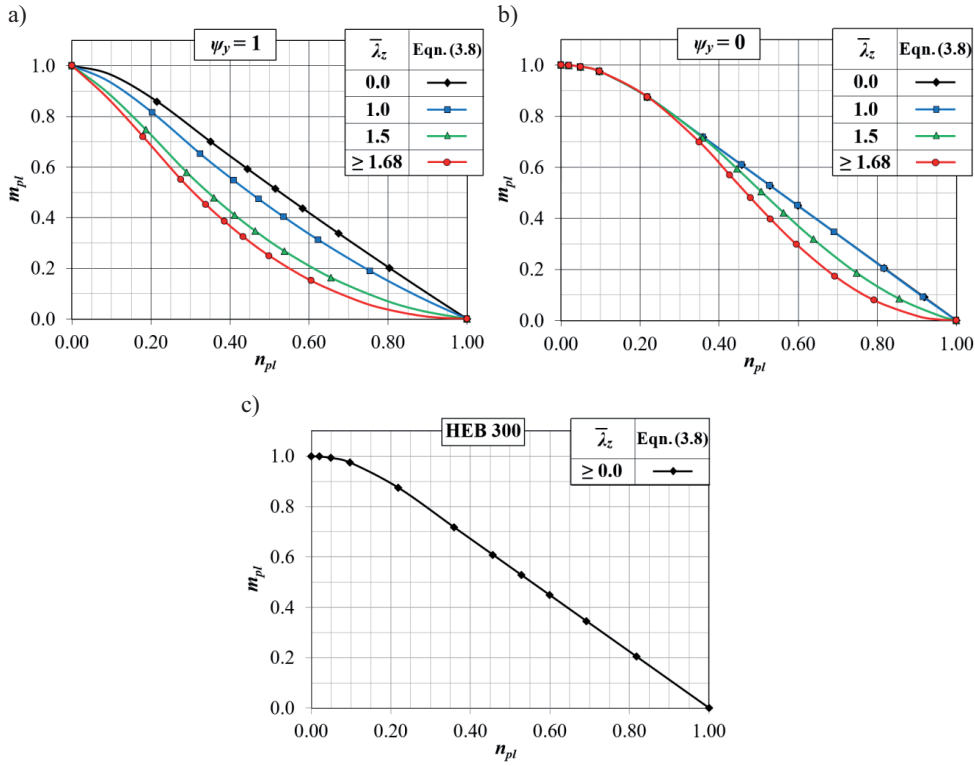

Fig. 15. Analytical in-plane resistance curves for: a) SMY [10], b) TMY, c) AMY

3.3 Flexural-torsional reduction factor by General Method

For each value of the action effects ratio, the results presented in Figs. 9 and 15a are used to calculate $\chi_{FT} = s_b / s_{pl}^{II}$ for the case of SMY, in Figs. 10 and 15b are used for the case of TMY and in Figs. 11 and 15c for the case of AMY. Each discrete value of χ_{FT} corresponds to particular slenderness ratio $\bar{\lambda}_{FT} = \sqrt{s_{pl}^{II} / s_{cr}}$ calculated with use of the results presented in Figs. 12 and 15a are used to calculate $\bar{\lambda}_{FT} = \sqrt{s_{pl}^{II} / s_{cr}}$ for the case of SMY, in Figs. 13 and 15b for the case of TMY and in Figs. 14 and 15c for the case of AMY. All pairs of (χ_{FT}, $\bar{\lambda}_{FT}$) are plotted respectively in Fig. 16 for SMY, Fig. 17 for TMY and Fig. 18 for AMY.

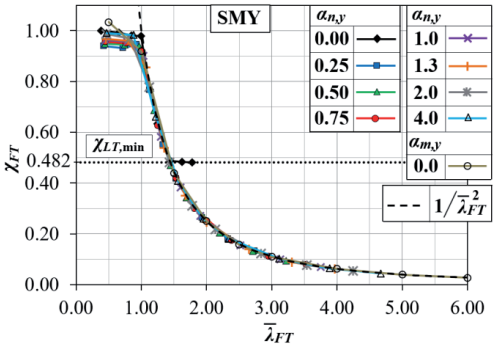

Fig. 16. Numerical FTB curves in FT coordinates for the case of SMY [10]

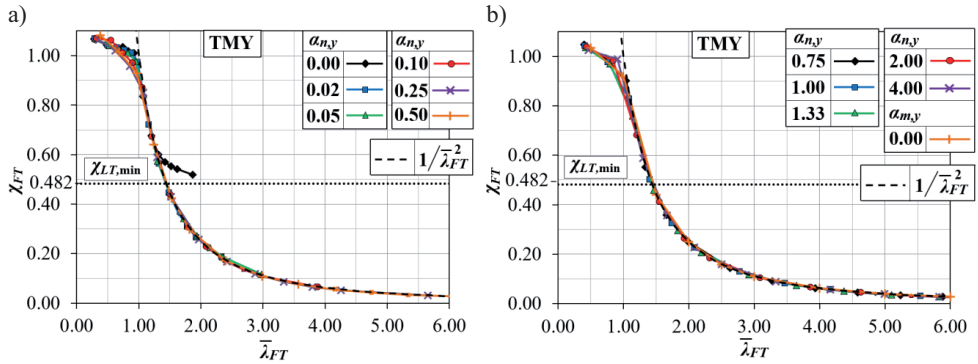

Fig. 17. Numerical FTB curves in FT coordinates for the case of TMY

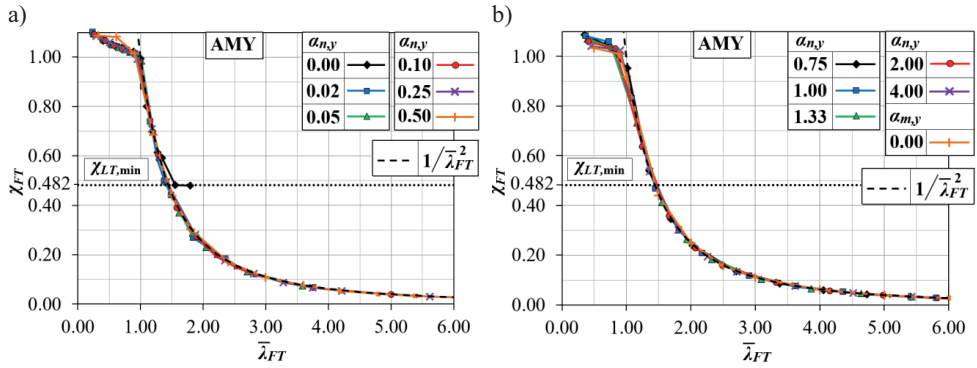

Fig. 18. Numerical FTB curves in FT coordinates for the case of AMY

The following conclusions can be drawn:

1. Buckling curves in the FT coordinates presented in Figs. 16-18 are more general than those in the LT coordinates presented in Figs 4, 5 and 7.

2. In the case of the flexural minor axis buckling with zero contribution of the bending moment ($\alpha_{m,y} = 0$) the buckling curves in Figs 4, 5 and 7 reduce to the abscissa straight line while in Figs. 16-18 the FTB curves for the $\bar{\lambda}_{FT} > 1$ reduce to the elastic buckling hyperbola.

3. For $\bar{\lambda}_{FT} > 1$, the FTB resistance decreases rapidly and the results are practically equal to elastic buckling hyperbola $\chi_{FT} = 1/\bar{\lambda}_{FT}^2$. For the $\bar{\lambda}_{FT} \leq 1$, the numerical GMNA+ results are placed close to unity representing the full yielding of the element most stressed section under a given combination of stress resultants.

2. In all the values of the gradient moment ratio considered and the case of bending without compression ($\alpha_{n,y} = 0$) for approximately $\bar{\lambda}_{FT} > \sqrt{M_{y,pl}/M_{z,pl}} = 1.44$, the buckling resistance reduction factor starts to approach the constant value of $\chi_{LT,min} = M_{z,pl}/M_{y,pl} = 0.482$.

4. FINAL REMARKS AND CONCLUSIONS

It has been proven that regardless of the moment gradient ratio, the GM buckling resistance reduction factor of quasi-straight and residual stress free beam-columns may be represented, except for the values for low beam-columns slenderness ratio $\bar{\lambda}_{FT}$, by the elastic buckling hyperbola $1/\bar{\lambda}_{FT}^2$. It has been showed that only in the case of bending without compression ($\alpha_{n,y} = 0$), the buckling resistance reduction factor for $\bar{\lambda}_{FT} > \sqrt{M_{y,pl}/M_{z,pl}}$ starts to approach the constant value of $\chi_{LT,min} = M_{z,pl}/M_{y,pl}$. This confirmed that the large twist rotation affects the resistance of very slender beams by increasing the resistance above that resulting from the elastic buckling hyperbola. This factor might be considered as negligible when the major axis bending moment is accompanied by an axial compressive force. In summary, the FTB reduction factor for quasi-straight prismatic beam-columns under considered load cases may be approximated analytically in the following way:

(4.1a) $$\chi_{FT} = \frac{s_{b,FT}}{s_{pl}^{II}} = 1 \quad \text{for} \quad \bar{\lambda}_{FT} \leq 1$$

(4.1b) $$\chi_{FT} = \frac{s_{b,FT}}{s_{pl}^{II}} = \frac{1}{\bar{\lambda}_{FT}^2} \quad \text{for} \quad \bar{\lambda}_{FT} > 1$$

(4.1c) $$\chi_{FT} = \frac{s_{b,FT}}{s_{pl}^{II}} = \chi_{LT,min} = \frac{M_{z,pl}}{M_{y,pl}} \quad \text{for} \quad \bar{\lambda}_{FT} > \sqrt{\frac{M_{y,pl}}{M_{z,pl}}} \text{ and } \alpha_{n,y} = 0$$

Eurocode design rules [6] are based on the imperfect member model. The presented herein GM concept considers only a disturbance to perfect geometry (GMNA+) in the form of the lowest buckling mode with infinitesimally small amplitude that produce the initial configuration corresponding to the quasi-perfect initial state. Results presented in this study show the general behaviour of beam-columns and they might be useful for the refinement of GM in order to include the effect of a non-zero residual resistance of slender beam-columns.

REFERENCES

1. ABAQUS Theory manual, Version 6.11, Dassault Systèmes, 2011.
2. ABAQUS/Standard User's manual, Version 6.11, Dassault Systèmes, 2011.
3. A.M. Baptista, "Resistance of steel I-sections under axial force and biaxial bending", Journal of Constructional Steel Research 72: 1-11, 2012.
4. F. Bijlaard, M. Feldmann, J. Naumes, G. Sedlacek, "The "general method" for assessing the out-of-plane stability of structural members and frames and the comparison with alternative rules in EN 1993 – Eurocode 3 – Part 1-1", Steel Construction 3: 19-33, 2010.
5. J. Bonet, R.D. Wood, "Nonlinear continuum mechanics for finite element analysis", second ed., Cambridge: Cambridge University Press, 2008.
6. Eurocode 3. PN-EN 1993-1-1: 2006 Design of steel structures, Pat 1-1: General rules and rules for buildings, PKN, Warsaw, 2006.
7. J. Ferreira, P. V. Real, C. Couto, "Comparison of the General Method with the Overall Method for the out-of-plane stability of members with lateral restraints", Engineering Structures 151: 153-172, 2017.
8. M.A. Gizejowski, Z. Stachura, R.B. Szczerba, M.D. Gajewski, "Buckling resistance of steel H-section beam-columns: In-plane buckling resistance", Journal of Constructional Steel Research 157: 347-358, 2019.
9. M.A. Gizejowski, Z. Stachura, R.B. Szczerba, M.D. Gajewski, "Out-of-plane buckling resistance of rolled steel H-section beam-columns under unequal end moments", Journal of Constructional Steel Research 160: 153-168, 2019.
10. M.A. Gizejowski, Z. Stachura, M.D. Gajewski, R.B. Szczerba, "Effects of large displacements on the flexural-torsional buckling resistance of steel H-section beam-columns", in A. Zingoni (ed.), Advances in Engineering Materials, Structures and Systems: Innovations, Mechanics and Applications, London: Taylor & Francis Group, 848-853, 2019.
11. M.A. Gizejowski, R.B. Szczerba, M.D. Gajewski, Z. Stachura, "Buckling resistance criteria of prismatic beams under biaxial moment gradient", International Journal of Steel Structures 19: 559-576, 2019.
12. M. Hosseini, H. Abbas, "Strain hardening in M–P interaction for metallic beam of I-section", Thin-Walled Structures 62: 243-256, 2013.
13. S. Jemiolo, M. Gajewski, "Hyperelasto-plasticity", Warsaw: Warsaw University of Technology Publishing House, 2017 (in Polish).
14. M. Nedelcu, "Generalisation of the Ayrton-Perry formula for the global-distortional-local buckling of thin-walled members", Thin-Walled Structure 118: 73-86, 2017.
15. F. Papp, A. Rubert, J. Szalai, "DIN EN 1993-1-1 based integrated stability analysis of 2D/3D steel structures", Stahlbau, Part 1 – 83 (1): 1-15, 2014; Part 2 – 83 (2): 122-141, 2014; Part 3 – 83 (5): 325-342, 2014 [in German].
16. I.M.J. Rombouts, H.H. Snijder, R.W.A. Dekker, P.A. Teeuwen, "Resistance to moment-normal force interaction of I-shaped steel sections", Journal of Constructional Steel Research 127: 28-40, 2016.
17. L. Simoes da Silva, L. Marques, C. Rebelo, "Numerical validation of the general method in EC3-1-1 for prismatic members", Journal of Constructional Steel Research 66: 575-590, 2010.
18. L. Simoes da Silva, R. Simoes, H. Gervasio, "Design of steel structures, Eurocode 3: Design of steel structures, Part 1-1: General rules and rules for buildings", second ed., ECCS Eurocode Design Manual, Berlin: Ernst & Sohn, 2016.
19. L. Simoes da Silva, T. Tankova, L. Marques, U. Kuhlmann, A. Kleiner, J. Spiegler, H.H. Snijder, R.W.A. Dekker, A. Taras, N. Popa, "Safety assessment across modes driven by plasticity, stability and fracture". In 8th European Conference on Steel and Composite Structures (EUROSTEEL 2017), Copenhagen, Denmark, 3689–3698, 2017.

20. E.A. de Souza Neto, D. Peric, D. R. J. Owen, "Computational methods for plasticity: theory and applications", John Wiley & Sons Ltd, 2008.
21. J. Szalai, F. Papp, "On the theoretical background of the generalization of Ayrton-Perry type resistance formulas", Journal of Constructional Steel Research 66 (5): 670-679, 2010.
22. J. Szalai, "Complete generalization of the Ayrton-Perry formula for beam-column buckling problems", Engineering Structures 153: 205-223, 2017.
23. T. Tankova, L. Marques, A. Andrade, L. Simoes da Silva, "A consistent methodology for the out-of-plane buckling resistance of prismatic steel beam-columns", Journal of Constructional Steel Research 128: 839-852, 2017.
24. A. Taras, "Contribution to the development of consistent stability design rules for steel members", PhD thesis, Technical University of Graz; Graz, Austria, 2011.
25. N.S. Trahair, M.A. Bradford, D. A. Nethercot, L. Gardner, "The behaviour and design of steel structures to EC3". Second ed. London-New York: Taylor and Francis, 2008.
26. W. Wojewódzki: "Nośność graniczna konstrukcji prętowych", Warsaw: Warsaw University of Technology Publishing House, 2012 (in Polish).
27. X. Yun, L. Gardner, N. Boissonnade, "Ultimate capacity of I-sections under combined loading – Part 2: Parametric studies and CSM design", Journal of Constructional Steel Research 148: 265-274, 2018.

Appendix: Buckling modes for AMY and TMY loading cases

The lowest overall buckling modes for specified dimensional n and m_y values:

Moment antisymmetrical (AMY) and axial compression	Moment triangular (TMY) and axial compression
$n = 0$ – LT mode corresponding to the antisymmetric moment diagram 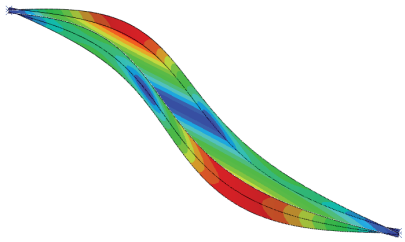	$n = 0$ – LT mode corresponding to the triangular moment diagram 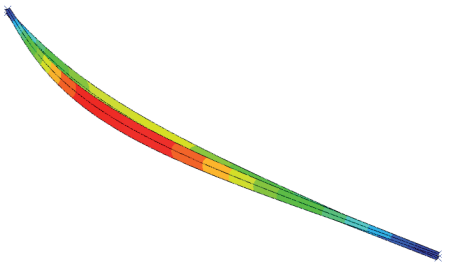
$n/m_y = 0.01$ 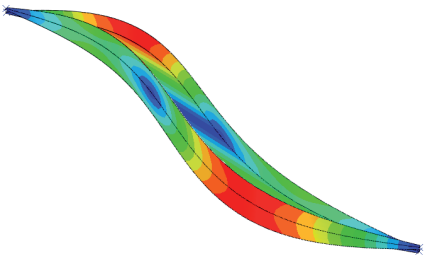	$n/m_y = 0.01$ 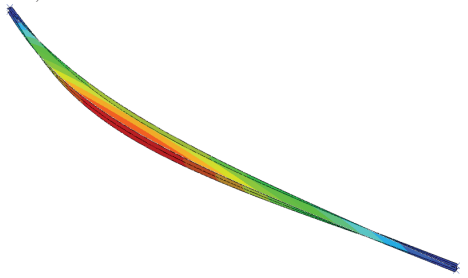

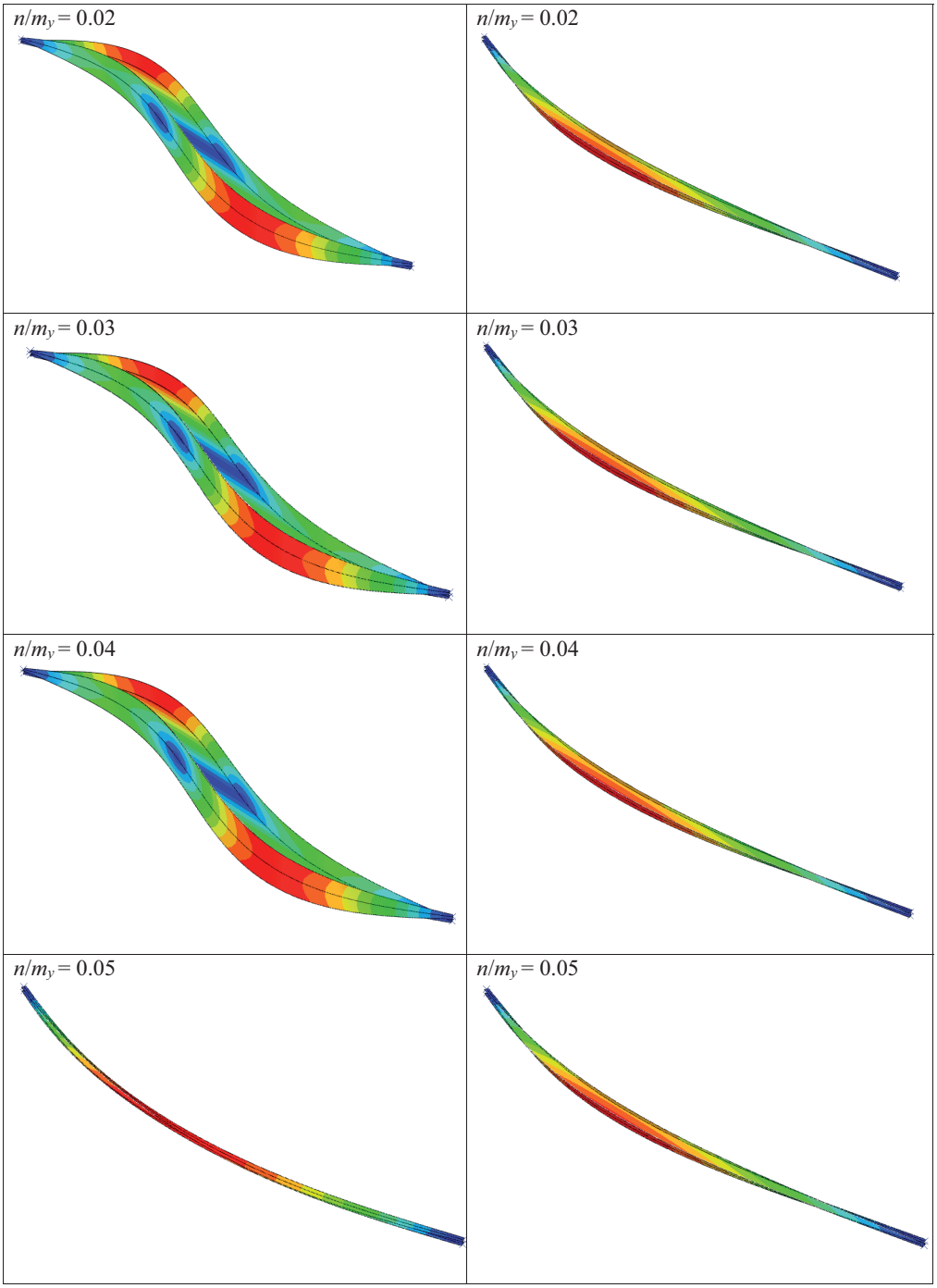
$n/m_y = 0.02$
$n/m_y = 0.02$
$n/m_y = 0.03$
$n/m_y = 0.03$
$n/m_y = 0.04$
$n/m_y = 0.04$
$n/m_y = 0.05$
$n/m_y = 0.05$

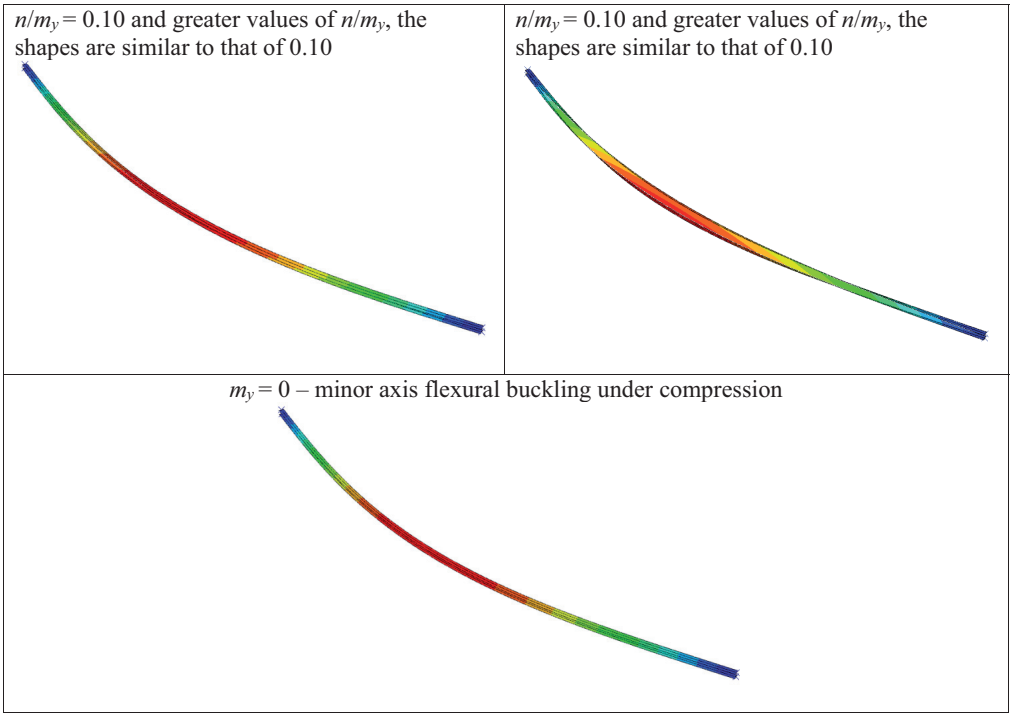

LIST OF FIGURES AND TABLES:

WYBOCZENIE POZORNIE PROSTYCH ELEMENTÓW DWUTEOWYCH SZEROKOSTOPOWYCH, ŚCISKANYCH I ZGINANYCH MOMENTAMI PODPOROWYMI O RÓŻNYCH WARTOŚCIACH I ZNAKU

Słowa kluczowe: metoda ogólna, duże przemieszczenia, wyboczenie giętno-skrętne, stalowe walcowane przekroje dwuteowe szerokostopowe, elementy ściskane i zginane

STRESZCZENIE:

Dwuteowniki stalowe o przekroju bisymetrycznym, poddawane ściskaniu i zginaniu względem głównej osi bezwładności przekroju, są wrażliwe na wyboczenie względem osi mniejszej bezwładności, przy jednoczesnej podatności na deformacje zgięciowe i skręcenie względem tej osi bezwładności. Analizy numeryczne wykazały, że w sytuacji, kiedy na końcach elementu quasi-idealnego występuje obciążenie podporowymi momentami zginającymi, wrażliwość na wyboczenie giętno-skrętne zależy w głównej mierze od stosunku momentów bezwładności analizowanego przekroju oraz dodatkowo zależy, i to w sposób istotny, od gradientu momentu względem głównej osi bezwładności przekroju. W przypadku zginania względem przekrojowej głównej osi bezwładności (osi *y-y*) z udziałem siły ściskającej, nawet o bardzo małej wartości w porównaniu z siłą powodującą uplastycznienie (równą nośności przekroju klasy 1 na ściskanie), następuje drastyczna redukcja nośności elementów o typowo konstrukcyjnych długościach. Na podstawie przeprowadzonych obliczeń można zaobserwować, że wyboczenie następuje wskutek zginania w płaszczyźnie mniejszej bezwładności przekroju, któremu towarzyszą znaczne skręcenia przekroju. W miarę wzrostu wartości współczynnika obciążenia, który definiujemy jako stosunek bezwymiarowej siły osiowej do bezwymiarowego maksymalnego momentu zginania względem osi większej bezwładności, następuje oddalanie się krzywej wyboczeniowej od tej dla wyboczenia giętno-skrętnego i zbliżenie się do krzywej dla wyboczenia względem osi mniejszej bezwładności. W niniejszej pracy przeanalizowano wpływ wybranych czynników na nośność przy wyboczeniu giętno-skrętnym typowego elementu stalowego, definiowaną w ujęciu tzw. eurokodowej metody ogólnej, rozwijanej przez autorów w innych pracach. Do analiz parametrycznych wykonywano metodę elementów skończonych (MES).

W uwagi na fakt, że w wypadku rozważanych elementów ściskanych i zginanych, zwichrzeniu oraz wyboczeniu giętno-skretnemu w sytuacji małego udziału podłużnej siły ściskającej, towarzyszy zwykle znaczny obrót przekroju, wszystkie analizy MES wykonano w ramach teorii umiarkowanie dużych deformacji, tj. wprowadzając logarytmiczną miarę odkształcenia i tensor naprężeń Kirchhoffa. Nie jest to formalnie teoria dowolnych deformacji, tylko płynne przejście z teorii małych odkształceń do teorii dużych deformacji, co w przypadku analizowanych zagadnień jest przybliżeniem wystarczająco dokładnym. W rozwiązywanych zagadnieniach utraty stateczności, elementy ściskane i zginane są modelowane przy zastosowaniu elementów powłokowych SR ze zredukowanym całkowaniem. Przyjęto sprężysto-plastyczny model materiału z warunkiem plastyczności Hubera-Misesa i stowarzyszonym z nim prawem płynięcia. Uwzględniono izotropowe wzmocnienie odkształceniowe.

W niniejszej pracy analizowany jest wpływ smukłości elementu, wpływ rozkładu momentu na długości elementu (wykres momentu stały, trójkątny i antysymetryczny) oraz wpływ stosunku znormalizowanej siły ściskającej do znormalizowanego momentu zginającego. Ostateczne wnioski i wyniki symulacji numerycznych są odniesione do sformułowań analitycznych, w tym eurokodowej metody ogólnej, odnoszącej się do definiowania nośności elementów ulegających wyboczeniu giętno-skrętnemu. W pracy wykazano, że niezależnie od rozkładu momentu zginającego względem głównej osi bezwładności przekroju *y-y*, redukcja nośności elementu quasi-idealnego bez naprężeń wstępnych, za wyjątkiem elementów o bardzo niskiej smukłości, może być określony przez hiperbolę wyboczenia giętno-skrętnego,

a więc w sposób analogiczny do sprężystego wyboczenia eulerowskiego. Zaobserwowano, że znaczne obroty przekroju wpływają istotnie na nośność elementów o bardzo dużej smukłości, podnosząc ich nośność ponad przewidywaną hiperbolą wyboczenia sprężystego. Efekt ten może być pominięty wówczas, gdy zginaniu względem osi większego momentu bezwładności towarzyszy siła ściskająca. Wykazano, że jedynie przy zginaniu bez udziału ściskającej siły podłużnej, wskaźnik redukcji nośności elementów smukłych zbliża się do stałej wartości równej $\chi_{LT,min} = M_{z,pl}/M_{y,pl}$ .W podsumowaniu artykułu podano wzory analityczne, pozwalające na określenie współczynników redukcyjnych w zależności od tego, czy występuje podłużna siła ściskająca, czy też nie. W wypadku występowania niezerowej wartości siły ściskającej wyróżniono dwa przedziały smukłości: $\chi_{FT} = \frac{s_{b,FT}}{s_{pl}^{II}} = 1$ przy $\bar{\lambda}_{FT} \leq 1$ oraz $\chi_{FT} = \frac{s_{b,FT}}{s_{pl}^{II}} = \frac{1}{\bar{\lambda}_{FT}^2}$ przy $\bar{\lambda}_{FT} > 1$. Z kolei w sytuacji, gdy zginaniu nie towarzyszy siła podłużna, występuje trzeci przedział smukłości, w którym obowiązuje stała relacja $\chi_{FT} = \frac{s_{b,FT}}{s_{pl}^{II}} = \chi_{LT,min} = \frac{M_{z,pl}}{M_{y,pl}}$.

Eurokodowe reguły projektowania konstrukcji stalowych są formułowane dla elementów z imperfekcjami. Prezentowana w niniejszej pracy koncepcja oceny nośności w ujęciu metody ogólnej dotyczy wyłącznie sytuacji, w której zaburzenia idealnej geometrii zadawane są w postaci najniższej formy własnej wyboczenia z amplitudą o najmniejszej możliwej wartości, która eliminuje osobliwość zadania (geometria quasi-idealna).

Wyniki i wnioski z analiz przedstawionych w niniejszej pracy mogą być w przyszłości w łatwy sposób wykorzystane do udoskonalenia metody ogólnej w kierunku uwzględnienia realnych imperfekcji geometrycznych i materiałowych (naprężeń własnych) w celu określenia projektowego współczynnika redukcyjnego do nośności wyboczeniowej, który uwzględnia efekt podwyższenia nośności smukłych elementów zginanych i ściskanych.

Received: 14.08.2020, Revised: 13.11.2020